View metadata, citation and similar papers at core.ac.uk

brought to you by CORE

provided by IntechOpen

# We are IntechOpen, the world's leading publisher of Open Access books Built by scientists, for scientists

**4,800**
Open access books available

**122,000**
International authors and editors

**135M**
Downloads

Our authors are among the

**154**
Countries delivered to

**TOP 1%**
most cited scientists

**12.2%**
Contributors from top 500 universities

CLARIVATE ANALYTICS BOOK CITATION INDEX INDEXED

WEB OF SCIENCE™

Selection of our books indexed in the Book Citation Index in Web of Science™ Core Collection (BKCI)

## Interested in publishing with us?
## Contact book.department@intechopen.com

Numbers displayed above are based on latest data collected.
For more information visit www.intechopen.com

Chapter

# Water Splitting Electrocatalysis within Layered Inorganic Nanomaterials

*Mario V. Ramos-Garcés, Joel Sanchez, Isabel Barraza Alvarez, Yanyu Wu, Dino Villagrán, Thomas F. Jaramillo and Jorge L. Colón*

## Abstract

The conversion of solar energy into chemical fuel is one of the "Holy Grails" of twenty-first century chemistry. Solar energy can be used to split water into oxygen and protons, which are then used to make hydrogen fuel. Nature is able to catalyze both the oxygen evolution reaction (OER) and the hydrogen evolution reaction (HER) required for the conversion of solar energy into chemical fuel through the employment of enzymes that are composed of inexpensive transition metals. Instead of using expensive catalysts such as platinum, cheaper alternatives (such as cobalt, iron, or nickel) would provide the opportunity to make solar energy competitive with fossil fuels. However, obtaining efficient catalysts based on earth-abundant materials is still a daunting task. In this chapter, we review the advancements made with zirconium phosphate (ZrP) as a support for earth-abundant transition metals for the OER. Our studies have found that ZrP is a suitable support for transition metals as it provides an accessible surface where the OER can occur. Further findings have also shown that exfoliation of ZrP increases the availability of sites where active species can be adsorbed and performance is improved with this strategy.

**Keywords:** water splitting, electrocatalysis, zirconium phosphate, inorganic nanomaterials, oxygen evolution

## 1. Introduction

Global energy consumption is projected to increase drastically in the coming decades [1]. To meet this demand, it is estimated that there are 1000–2000 years of fossil fuel resources [2]. Nonetheless, while fossil fuels could meet this huge demand of energy, $CO_2$ emissions from these resources would contribute to the recognized danger of climate change by increasing anthropogenic carbon emissions to the atmosphere. This motivates the development of sustainable energy production technologies, including fuel production, using solar energy in a process that has been called artificial photosynthesis. However, there are large scientific and technical challenges involved in these schemes.

One promising scheme for this purpose is the use of hydrogen as a fuel. Hydrogen has the largest energy density over any other fuel and it is the most abundant molecule in the universe. Hydrogen's energy density is 120 MJ/kg, more than twice than that of natural gas and almost three times higher than petroleum [3]. The problem with hydrogen is that even though it is very abundant, it is hard to obtain in pure form since it readily reacts with other substances and it is mostly found in compounds. Currently, ~96% of hydrogen is produced from fossil fuels with the steam methane reforming process [4]. Thus, methods for producing hydrogen from hydrogen-containing resources like biomass and water need to be more environmentally friendly and economical in order to substitute current methods of hydrogen production [4]. The high interest of hydrogen as a fuel arises because this gas is highly flammable, burns cleanly, and the cost of solar-based electricity is falling rapidly, including that used for hydrogen production [5]. The product of hydrogen combustion is water and energy, making this process extremely clean:

$$2H_2(g) + O_2(g) \rightarrow 2H_2O(g)\ \Delta H = -286\ \text{kJ/mol}$$

Out of all energy resources, solar energy is the most abundant, but it is an intermittent resource [6]. Therefore, to effectively use solar energy, we must convert and store it. One way to store this energy is in the form of chemical fuels, such as hydrogen. The idea is to split water in its components (hydrogen and oxygen) with the help of solar energy since 4.92 eV is stored when two water molecules are split [7]. This approach to store energy in the form of chemical bonds (a process that mimics the natural photosynthetic process) is called artificial photosynthesis. An example of artificial photosynthesis is the process occurring in a solar fuel cell. In such cells water is split using sunlight as the energy source. This reaction involves two separate redox reactions, one being the oxidation of water to produce oxygen and protons (a 4-electron process) and the other one is the reduction of protons to form dihydrogen:

$$\text{Water oxidation: } 2H_2O \rightarrow O_2 + 4H^+ + 4e^- \ (\text{Oxygen evolution reaction, OER}).$$

$$\text{Proton reduction: } 2H^+ + 2e^- \rightarrow H_2 \ (\text{Hydrogen evolution reaction, HER}).$$

Electrochemical water splitting can be achieved by using devices that can harvest the sun's energy. The two main configurations of these devices consist of (1) a photovoltaic (PV) device connected to a separate electrolyzer with catalysts that drive the necessary half reactions (PV/electrolysis) and (2) a fully integrated system where the catalysts are deposited on top of the light absorbing materials (photoelectrochemical, PEC devices) [8]. The efficiency of these devices is calculated based on the solar-to-hydrogen (STH) or solar-to-fuel (STF) efficiency, which is defined as the amount of chemical energy produced in the form of fuel divided by the solar energy input, with no external bias applied [9]. High STH efficiencies are desired as it has been proved that it is the factor with the biggest impact on the final cost of the fuel produced on any of these systems [8]. Although, other factors such as stability and material cost are also important for the final cost of the fuel.

Theoretical efficiencies calculated using combinations of published catalysts for the OER and the HER in a PEC device show that the STH efficiencies are far lower than the maximum thermodynamically achievable efficiency of 41% [8]. This highlights the need to develop more active catalysts, especially for the OER

as it is the main cause of energy loss in the form of kinetic overpotentials during fuel production. Furthermore, to bring these technologies towards economical implementation, it is of much importance to continually improve device performance. Besides, benchmarking studies have shown that catalyst stability is also a major issue as the reactions are mostly carried in harsh chemical conditions, especially in very high or low pH [10–12]. Recently, density functional theory (DFT) calculations have shown that performing the OER in a confined nanoscopic environment improves the electrochemistry of the reaction by lowering the overpotential and increasing the catalytic efficiency by 10% [13]. These theoretical results were modeled on a layered $RuO_2$ system and attributed the improvement in activity to interactions of intermediates with the opposite surface of the metal oxide. There is evidence that encapsulation of catalysts can lead to improvements on selectivity and activity for a variety of reactions, including water oxidation [14–17]. This motivated us to use the layered compound zirconium phosphate (ZrP) as a support for active OER catalysts to mimic an environment that theoretical works have modeled. We want to target the issues presented by OER catalysts by developing catalytic systems based on ZrP nanomaterials with the goal of optimizing efficiencies of future solar water splitting devices.

### 1.1 Zirconium phosphates

Zirconium phosphates are part of the group of water-insoluble phosphates of tetravalent metals containing layered structures. Zirconium bis(monohydrogen orthophosphate) monohydrate ($Zr(O_3POH)_2{\cdot}H_2O$, $\alpha$-ZrP) is the most extensively studied phase of ZrP. $\alpha$-ZrP has an interlayer distance of 7.6 Å with a layer thickness of 6.6 Å (**Figure 1a** and **b**) [18]. $\alpha$-ZrP has a structure in which the zirconium atoms in each layer align nearly to a plane with bridging phosphate groups located alternately above and below the metal atom plane [19]. Three oxygen atoms of the phosphate group bond to three different $Zr^{4+}$ and each $Zr^{4+}$ ion coordinates with oxygens from six different phosphate groups [19]. The fourth oxygen from the phosphate group, which has a proton, points towards the interlayer region and the surface of the nanoparticles. This proton can be exchanged with cations or molecules. The structure of $\alpha$-ZrP contains a zeolitic cavity in the interlayer region with a diameter of 2.61 Å that is occupied by a water molecule [20, 21].

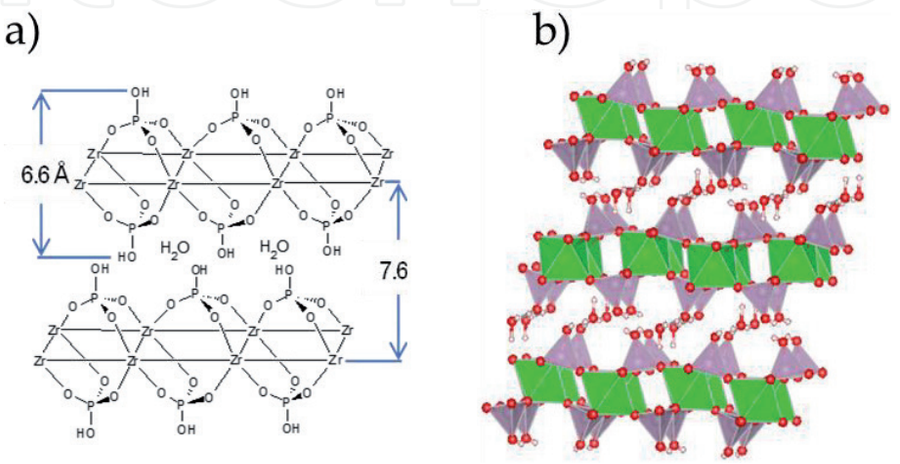


**Figure 1.**
*(a) The structure of α-ZrP. (b) Polyhedral model of the structure of α-ZrP.*

### 1.2 Intercalation of guest species into ZrP

Intercalation is defined as the reversible insertion of guest species into a lamellar host structure with maintenance of the structure features of the host [22]. For $\alpha$-ZrP, the direct intercalation of small cations is possible if they are smaller than 2.61 Å, but for larger cations and molecules intercalation is not significant and/or these species are exchanged at very slow rates [23–26]. To circumvent this problem, $\alpha$-ZrP pre-intercalated phases with sodium ions or n-butylammonium (both produce expanded phases) are commonly used as precursors to intercalate the intended guest species. One problem that arises with this method is that the pre-intercalated species do not necessarily exchange completely with the intended guest, thus becoming a contaminant in the intercalation product.

Martí and Colón developed a new direct intercalation method that does not require a pre-intercalation step using a highly hydrated phase of zirconium phosphate, θ-ZrP [27]. θ-ZrP maintains the $\alpha$-ZrP-type layered structure (**Figure 2**) but has an interlayer distance of 10.4 Å and has six water molecules per formula unit, in contrast with $\alpha$-ZrP that only has one [28]. Zirconium bis(monohydrogen orthophosphate) hexahydrate (θ-ZrP) converts back to $\alpha$-ZrP when it dehydrates. X-ray powder diffraction (XRPD) can be used to distinguished between both ZrP phases. When θ-ZrP is dried, producing $\alpha$-ZrP, the first diffraction peak at 2θ = 8.6° which corresponds to the 002-plane reflection of ZrP and that of the interlayer distance, shifts towards 11.6°; the angle corresponding to an interlayer distance of 7.6 Å, characteristic of $\alpha$-ZrP (**Figure 3**). For this reason, if a dry intercalation product is analyzed by XRPD and the first diffraction peak corresponds to a distance greater than 7.6 Å, this indicates that the intercalation reaction was successful [29]. One of three possible patterns can be observed by XRPD for intercalation products of ZrP; either (i) a pattern with a peak corresponding to a larger interlayer spacing at lower 2θ values than 11.6° indicates that the intercalant was introduced into the interlayer, (ii) a pattern with two distinct peaks, one at 2θ = 11.6° and one that appears at lower

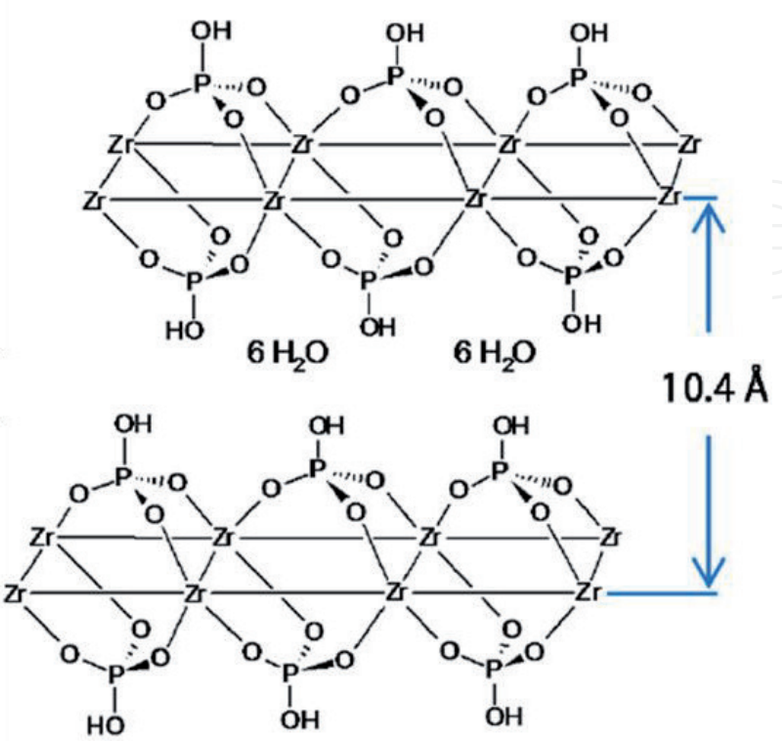


**Figure 2.**
*The structure of θ-ZrP.*

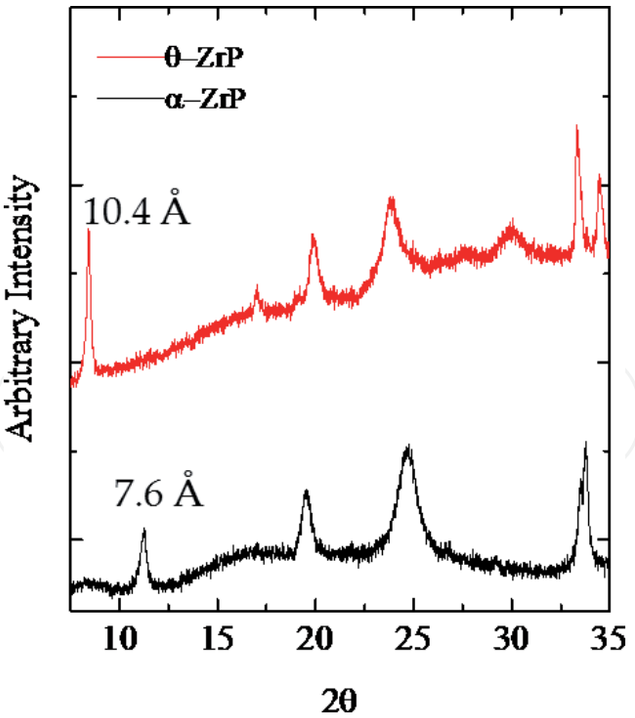


**Figure 3.**
*XRPD patterns of α-ZrP (black) and θ-ZrP (red).*

2θ values than 11.6° indicates that a mixed phase is present [30], and (iii) a pattern with no change in the reference peak, indicating that the intercalant species did not intercalate and is adsorbed on the outer surface of the layered structure or that is not present at all.

ZrP has been used for the intercalation of several photo-, bio- and redox-active compounds for a wide variety of applications including artificial photosynthesis, amperometric biosensors, and drug delivery [27, 30–42]. Even though ZrP has previously been studied for catalysis [43–47], membrane composites for proton exchange water electrolyzers [48–52], and as additive for catalytic layers for OER in order to protect metal oxide catalysts [53], our work is, to the best of our knowledge, the first time ZrP is used as an inorganic support for catalysts for the OER.

### 1.3 Chemical exfoliation of ZrP nanoparticles

The process of separating the layers of a layered material is known as exfoliation. This process has been extensively studied for a myriad of layered materials and the two-dimensional materials (2D) that result have been shown to have several advantages over their bulk systems [54]. *α*-ZrP has been successfully exfoliated through a variety of methods [55–58], and its nanosheets used for different applications [59–62]. The main strategy for ZrP exfoliation consists on the intercalation of small amines with positive charges that can easily displace the protons from the phosphate groups in an acid-base reaction and enter the interlayer space. If a high enough concentration of these amines is used, an amine double layer will form in the interlayer space, leading to exfoliation due to cation-cation repulsions (**Figure 4**) [56].

One of the most highly used amines for the exfoliation of ZrP is tetra-*n*-butylammonium hydroxide ($TBA^+OH^-$). If $TBA^+OH^-$ is used, the exfoliated material will consist of single nanosheets of ZrP suspended with $TBA^+$ attached to them. This reaction is temperature sensitive as it has been found that that hydrolysis of the ZrP edges occurs due to the $OH^-$ ions. However, the rate of hydrolysis of ZrP during exfoliation with $TBA^+OH^-$ at 0 °C is essentially zero [58]. If the exfoliated material

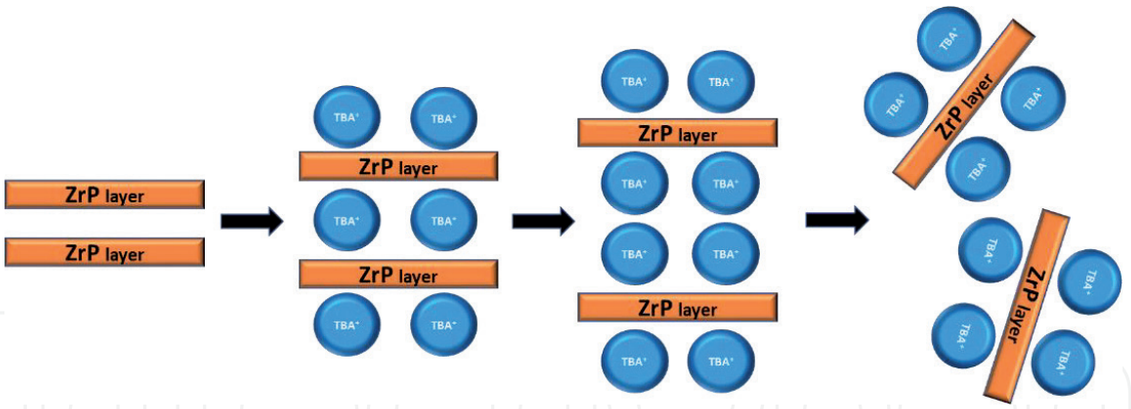


**Figure 4.**
*Schematic drawing of the ZrP exfoliation process with $TBA^+$.*

is dried, restacking of the layers occurs with a new expanded phase of 16.8 Å corresponding to $TBA^+$ intercalated in ZrP [63]. The $TBA^+$ cations can be displaced with another cationic species if the latter is put in contact with a suspension of the exfoliated ZrP nanoparticles. Hence, if the desired material is the exfoliated nanosheets with their phosphate groups protonated, then a follow up reaction with an acid can be performed [60].

## 2. Metal-modified ZrP based electrocatalysts for the OER

To facilitate the economic viability of water splitting, the efficiency of electrolyzers must be improved by addressing the overpotential losses associated with the sluggish OER kinetics. To this end, recent studies have focused on developing catalysts materials using earth-abundant transition metals [64]. Significant research has been devoted to improving OER electrocatalysts by using a wide variety of strategies that either increase the intrinsic activity of active sites or by increasing the number of them [65]. One general strategy that has been effective is to support active materials onto supports that engender improved performance [65–68]. ZrP properties make it a potential candidate as a support for active OER catalysts. Its ability to confine catalysts, high thermal stability, stability under a wide range of pH values, and its overall robustness are all desired for an ideal support. In our work, we intercalated the earth-abundant transition metal cations $Fe^{2+}$, $Fe^{3+}$, $Co^{2+}$, and $Ni^{2+}$ into ZrP and assessed these composite materials as OER electrocatalysts [69].

### 2.1 Metal-intercalated and surface adsorbed ZrP systems

To intercalate the desired transition metals, a suspension of θ-ZrP must be mixed with a solution of the metal salt precursor and left stirring for 5 days so that ion-exchange reaches equilibrium. To optimize metal loading for improved catalysis performance, we synthetized these composite materials with several synthesis metal salt:ZrP molar ratios (10:1, 5:1, 3:1, 1:1, 1:3, 1:5, 1:10, and 1:20 M:ZrP). A stepwise process is expected as a function of intercalant solution molarity; the intercalation reaction initiates from the edges of the particle and proceeds by diffusion of the metal cations towards the interior of the interlayer sheets [70]. The XRPD patterns (**Figure 5a**) for all four metal samples show that the first diffraction peak of ZrP is shifted to lower 2θ angles, indicating larger interlayer distances and successful intercalation. Increasing the M:ZrP molar ratios results in peak broadening and shifting in all samples indicating a more mixed phase is present and that the

layered structure has not achieved its maximum cation loading within the interlayer. However, at the highest loadings (i.e., 1:1–10:1 molar ratios), the original peak at 2θ = 11.6° disappeared, and a new peak emerged at significantly lower values of 2θ, reaching a final value indicative of the maximum interlayer distance for that particular metal cation intercalated within ZrP. As expected, +2 cations produced intercalated products with the first diffraction peak at lower angles than those produced by +3 cations. Compared to α-ZrP, the maximum interlayer distance increase observed for +2 cations was 2 Å, while for +3 cations it was 0.6 Å (**Figure 5b**). This difference in the increase in interlayer distance between the divalent and trivalent metal cations can be attributed to the difference electrostatic forces within the layers, consistent with Coulomb's Law. Trivalent cations produced a smaller increase because of a stronger electrostatic attraction between the metal cation and the negatively charged ZrP layers.

Ion-exchange in ZrP occurs at the Brönsted acid groups (P-OH) which are also present at the surface of the nanoparticles. Hence, there is no way of preventing that the metal cations get adsorbed to the surface. To obtain more insights into the nature of the activity of the samples, a metal-modified ZrP system in which the metals are only adsorbed onto the surface of the nanoparticles was also prepared. To prepare these samples, α-ZrP must be used as the ZrP source as the metal cations are large enough to not intercalate into the interlayer. XRPD data shows that the interlayer distance of these dry sample remains that of α-ZrP, 7.6 Å (**Figure 5b**). The presence of the metals in these systems was confirmed by high resolution X-ray photoelectron spectroscopy (XPS). XPS was also used to determine the atomic concentration on both metal-modified ZrP systems, intercalated and adsorbed [69]. Due to the uptake of metal cations within the much larger area of the interlayers of ZrP rather than solely on the surface in the adsorbed case, XPS high resolution scans show that intercalated ZrP systems have higher atomic metal content when compared to adsorbed systems at similar M:ZrP ratios.

Another useful tool to characterize ZrP systems is Fourier transform infrared spectroscopy (FT-IR). α-ZrP has four characteristic bands associated

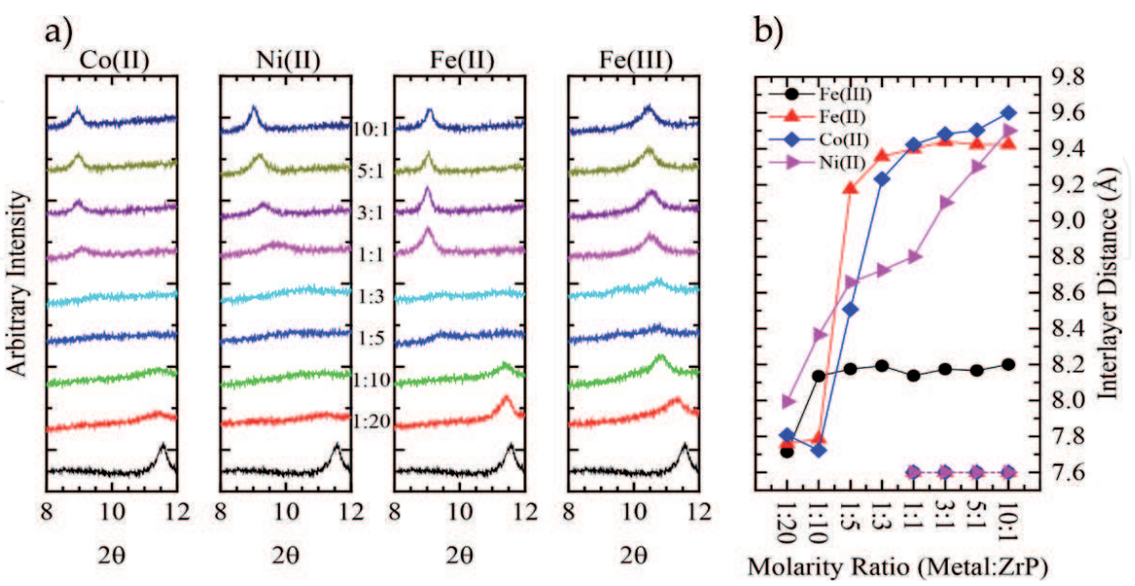


**Figure 5.**
*(a) XRPD patterns for Fe(II), Fe(III), Co(II), and Ni(II)-intercalated ZrP at (from top to bottom) 10:1, 5:1, 3:1, 1:1, 1:3, 1:5, 1:10, and 1:20 M:ZrP molar ratios. The bottom diffraction pattern in all frames is that of pure α-ZrP; (b) interlayer distance as a function of M:ZrP molar ratio for the various metal-intercalated ZrP materials. Metal-adsorbed systems are represented as dashed lines which have an exact interlayer spacing as pure α-ZrP indicating that metal intercalation did not occur. Taken from reference [69].*

with lattice water molecules. These bands appear at ~3600, ~3500, ~3140, and ~1600 $cm^{-1}$ [71]. When intercalation occurs, the intercalant species will displace interlayer water molecules. For this reason, bands associated with these water vibrational modes showed reduced relative intensity in the intercalated materials (**Figure 6a**). In contrast, metal-adsorbed samples showed very similar spectra to that of $\alpha$-ZrP, with the water bands still present, indicating negligible intercalation (**Figure 6b**). The characteristic orthophosphate group vibrations of ZrP are observed in the region of ~1100–950 $cm^{-1}$ (**Figure 6a**). Intercalated samples show a diminished relative intensity of the shoulder at the left part of the orthophosphate group vibrations at ~1050 $cm^{-1}$ that is attributed to the vibration of the exchangeable proton of the phosphate group, which is lost when the proton is exchanged by intercalation via ion exchange with other species. For metal-adsorbed samples, this vibration is still present indicating once again that no intercalation is observed.

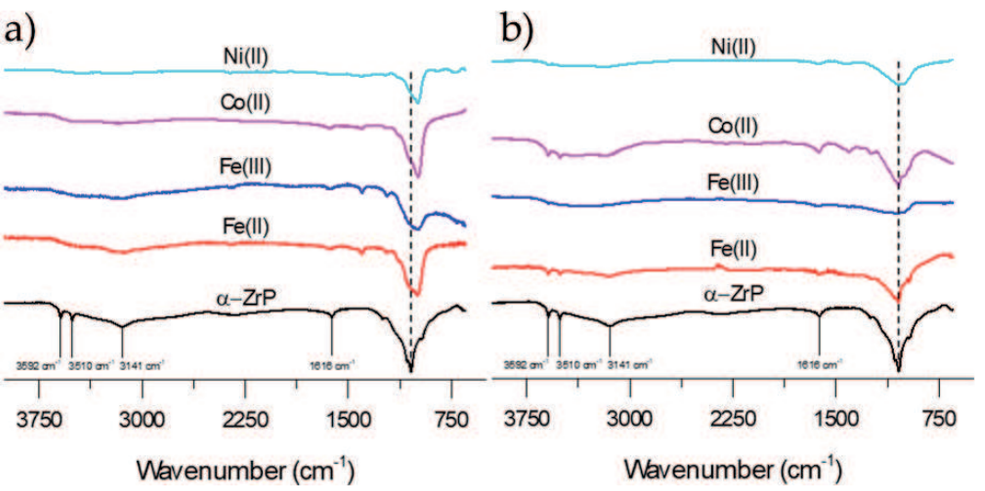


**Figure 6.**
*FTIR spectra of (a) intercalated and (b) adsorbed Fe(II), Fe(III), Co(II), and Ni(II) at 10:1 M:ZrP ratio. Taken from Ref. [69].*

## 2.2 OER electrochemical performance of metal-intercalated and surface adsorbed ZrP systems

To determine the activity of our metal-modified ZrP products towards the OER, cyclic voltammetry experiments were conducted using a Rotating Disk Electrode (RDE) assembly in alkaline electrolyte (0.1 M KOH). The methodology employed was according to the benchmarking protocols suggested for OER electrocatalysts [10–12]. The primary figure of merit from this data is the overpotential necessary to achieve 10 $mA/cm^2$ ($\eta_{j\ =\ 10\ mA/cm^2}$). The overpotential measured at 10 $mA/cm^2$ is the potential difference between the potential to achieve 10 $mA/cm^2$ and the thermodynamic potential of water oxidation (1.23 V vs. RHE). All samples were active for the OER, requiring between 0.5 and 0.7 V of overpotential to reach 10 $mA/cm^2$, depending on the choice of metal cation, the M:ZrP molar ratio used during synthesis, and whether the metal was intercalated into or adsorbed onto ZrP. In general, lower overpotentials are observed for the higher M:ZrP molar ratios, ascribed to higher metal loadings. Also, OER activities for the metal-adsorbed ZrP catalysts are greater than or equal to those of their metal-intercalated counterparts at the same loading, as seen by their lower overpotentials (**Figure 7**). This is

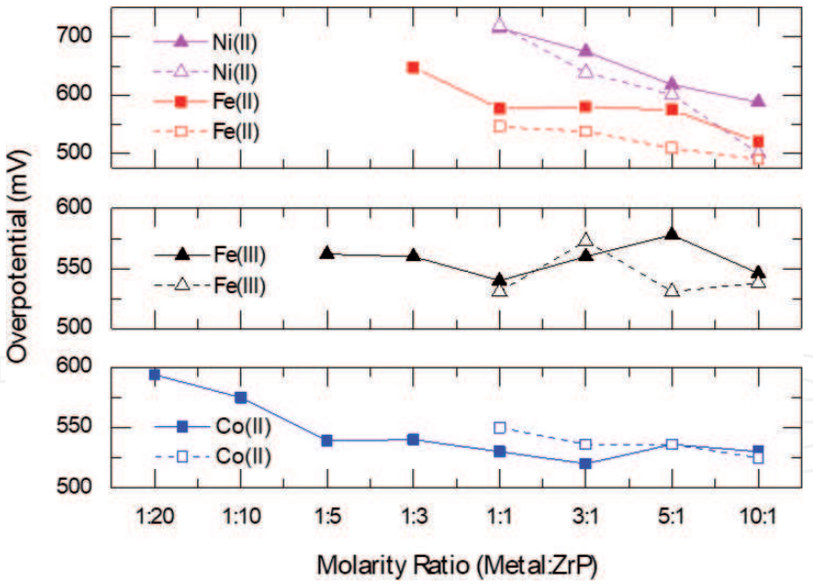


**Figure 7.**
*Electrochemical performance comparison of all four metal systems for adsorbed and intercalated species at 10 mA/cm² except for Ni(II) which was compared at 3 mA/cm². Solid and dashed lines represent intercalated and adsorbed metal ZrP systems, respectively. Taken from reference [69].*

somewhat surprising as XPS showed that higher metal loadings were achieved in the intercalated systems. This suggests that the OER is dominated by catalysis on the outer surface of the ZrP supported metal-based systems rather than within the layers, which may be limited by mass transport. These results serve as a basis for developing improved OER catalyst systems.

### 2.3 Metal-modified exfoliated ZrP

Our previous finding suggests that ZrP can serve as a support for transition metal-based OER catalysts and that the reaction occurs preferentially on the surface of the layered ZrP nanoparticles rather than the interlayer space [69]. Based on these results, we expected that exposing surface sites through exfoliation of ZrP could improve these catalytic systems. With the goal of developing more active materials, we prepared exfoliated ZrP nanosheets and modified these exfoliated nanoparticles with $Co^{2+}$ and $Ni^{2+}$ [72]. These systems underwent reaction at the same molar ratio than that of the best performing metal-adsorbed ZrP system (10:1 M:ZrP).

ZrP exfoliation was carried out by adding an excess of $TBA^+OH^-$ in an ice bath followed by an acid wash with HCl. To modify the exfoliated ZrP with the transition metals, an aqueous suspension of the nanosheets is put in contact with an aqueous solution of the metal salt precursor. The XRPD pattern of exfoliated ZrP shows the extreme broadening characteristic of successful exfoliation (**Figure 8**). The diffractograms of Co and Ni-modified ZrP nanosheets are very similar to that of exfoliated ZrP confirming that no further restacking occurs after metal modification (**Figure 8**). Transmission electron microscopy (TEM) also confirms this as the ZrP nanosheets show a fainter contrast when compared with $\alpha$-ZrP nanoparticles which is consistent with its thinner nature, since in TEM areas that contain heavy atoms or are thick appear darker (**Figure 9a–d**). After exfoliation, the nanosheets retain the hexagonal shape of $\alpha$-ZrP and no hydrated zirconia nanoparticles are observed decorating the edges of the sheets, indicating that the hydrolysis prone

edges were preserved by temperature control during the exfoliation reaction and that the structure of the layers did not change [58]. This was also confirmed by XPS as the P/Zr ratio after exfoliation remains constant at ~2.

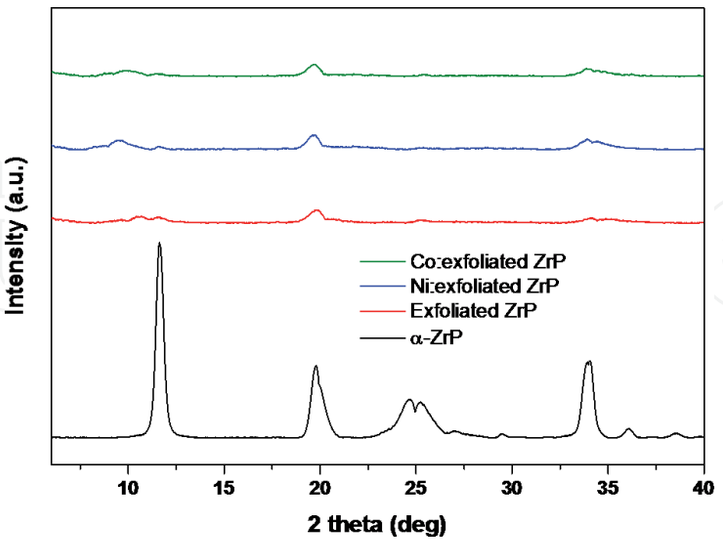


**Figure 8.**
*XRPD patterns of α-ZrP, exfoliated ZrP, and metal-modified exfoliated ZrP samples. Reprinted with permission from [72].*

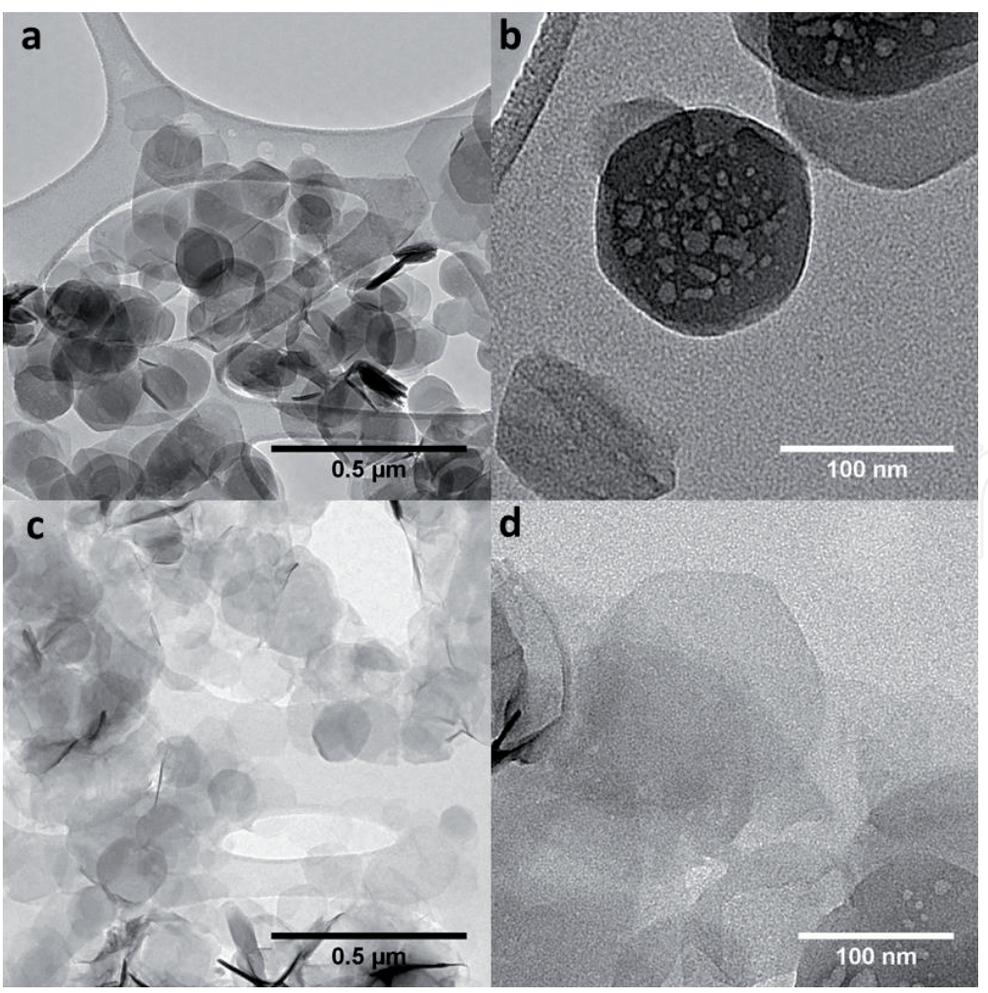


**Figure 9.**
*(a, b) TEM images of α-ZrP nanoparticles. Scale bar: 0.5 and 100 nm, respectively. (c, d) TEM images of exfoliated ZrP. Scale bar: 0.5 μm and 100 nm, respectively. Reprinted with permission from [72].*

### 2.4 OER electrochemical performance of metal-modified exfoliated ZrP electrocatalysts

Linear sweep voltammetry (LSV) was used to assess the activity of these exfoliated materials (**Figure 10**) [72]. OER catalytic currents for the exfoliated materials were shifted to lower potentials when compared to their surface adsorbed counterparts. The overpotential necessary to reach a current density of 10 mA/cm$^2$ for the Co-modified exfoliated nanosheets was 0.450 V, an improvement of 41 mV over the surface adsorbed Co material. For the Ni-modified the overpotential necessary to reach a current density of 3 mA/cm$^2$ is 0.410 V, an improvement of 181 mV over the surface adsorbed Ni material.

To elucidate the nature of the increased activity of the exfoliated materials, we determined the intrinsic activity of each catalytic site in both types of systems [72]. To construct a mass normalized current plot, we performed inductively plasma-mass spectrometry (ICP-MS) measurements on our samples to quantify the amount of nickel and cobalt metal content in the exfoliated and bulk materials. ICP-MS measurements show that the exfoliated samples are substantially better at adsorbing Co and Ni cations, leading to higher loadings than non-exfoliated ZrP. For our mass normalized plots, we assumed that all metal content quantified by ICP-MS

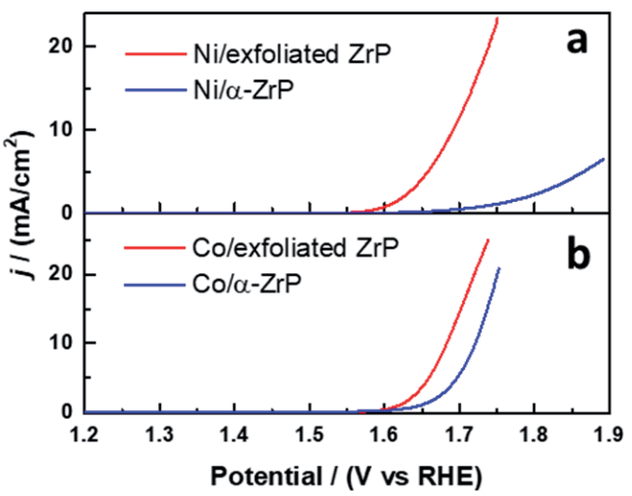


**Figure 10.**
*Linear sweep voltammograms of (a) Ni(II)/ZrP systems and (b) Co(II)/ZrP systems. Reprinted with permission from Ref. [72].*

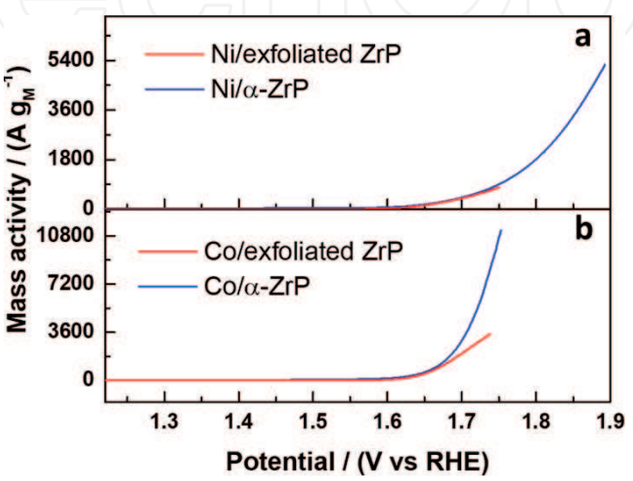


**Figure 11.**
*Mass normalized catalytic currents for (a) Ni(II)/ZrP systems and (b) Co(II)/ZrP systems. Reprinted with permission from Ref. [72].*

in the materials were active and accessible to perform OER. **Figure 11a** and **b** show the LSVs where the OER currents are normalized by the mass of the metal content. These exfoliated systems maintain reasonably high intrinsic activity values that, when coupled to a significant greater number of active sites leads to higher geometric activity. We concluded that the enhancement in activity is due to the fact that the inner layer surfaces are now more electrochemically accessible [72]. Through exfoliation the number of ion-exchange sites increases which increases the number of catalytic species that are distributed on the surface of zirconium phosphate, therefore giving rise to the improved performance.

## Acknowledgements

We would like to acknowledge the NSF Center for Chemical Innovation in Solar Fuels CHE-1305124 for funding these research efforts. M.V.R.-G. was also supported by the NSF-PREM Center for Interfacial Electrochemistry of Energy Materials (CiE2M) grant DMR-1827622.

## Conflict of interest

The authors declare no conflict of interest.

## Notes

M.V.R.-G. and J.L.C wrote the chapter. J.S., I.B.A., Y.W., D.V., and T.F.J. revised the work. All authors helped in the conception of the work, acquisition, analysis, and interpretation of the data.

## Author details

Mario V. Ramos-Garcés[1], Joel Sanchez[2], Isabel Barraza Alvarez[3], Yanyu Wu[3], Dino Villagrán[3], Thomas F. Jaramillo[2] and Jorge L. Colón[1*]

1 University of Puerto Rico at Río Piedras, San Juan, Puerto Rico, United States

2 Stanford University, Stanford, United States

3 University of Texas at El Paso, El Paso, United States

*Address all correspondence to: jorge.colon10@upr.edu

IntechOpen

© 2019 The Author(s). Licensee IntechOpen. This chapter is distributed under the terms of the Creative Commons Attribution License (http://creativecommons.org/licenses/by/3.0), which permits unrestricted use, distribution, and reproduction in any medium, provided the original work is properly cited. CC BY

## References

[1] Gray HB. Powering the planet with solar fuel. Nature Chemistry. 2009;**1**:7

[2] Lewis NS, Nocera DG. Powering the planet: Chemical challenges in solar energy utilization. Proceedings of the National Academy of Sciences of the United States of America. 2006;**103**:15729-15735

[3] Thomas G. Overview of Storage Development DOE Hydrogen Program [Internet]. Available from: http://www1.eere.energy.gov/hydrogenandfuelcells/pdfs/storage

[4] Cheng Y, Jiang SP. Advances in electrocatalysts for oxygen evolution reaction of water electrolysis-from metal oxides to carbon nanotubes. Progress in Natural Science: Materials International. 2015;**25**:545-553

[5] Bockris JO'M. Hydrogen no longer a high cost solution to global warming: New ideas. International Journal of Hydrogen Energy. 2008;**33**:2129-2131

[6] Solar Fuels. Lewis Research Group [Internet]. Available from: http://nsl.caltech.edu/home/solar-fuels

[7] Dempsey JL, Brunschwig BS, Winkler JR, Gray HB. Hydrogen evolution catalyzed by Cobaloximes. Accounts of Chemical Research. 2009;**42**:1995-2004

[8] Montoya JH, Seitz LC, Chakthranont P, Vojvodic A, Jaramillo TF, Nørskov JK. Materials for solar fuels and chemicals. Nature Materials. 2017;**16**:70-81

[9] Chen Z, Jaramillo TF, Deutsch TG, Kleiman-Shwarsctein A, Forman AJ, Gaillard R, et al. Accelerating materials development for photoelectrochemical hydrogen production: Standards for methods, definitions, and reporting protocols. Journal of Materials Research. 2010;**25**:3-16

[10] McCrory CCL, Jung S, Ferrer IM, Chatman SM, Peters JC, Jaramillo TF. Benchmarking hydrogen evolving and oxygen evolving electrocatalysts for solar water splitting devices. Journal of the American Chemical Society. 2015;**137**:4347-4357

[11] McCrory CCL, Jung S, Peters JC, Jaramillo TF. Benchmarking heterogeneous electrocatalysts for the oxygen evolution reaction. Journal of the American Chemical Society. 2013;**135**:16977-16987

[12] Jung S, McCrory CCL, Ferrer IM, Peters JC, Jaramillo TF. Benchmarking nanoparticulate metal oxide electrocatalysts for the alkaline water oxidation. Journal of Materials Chemistry A. 2016;**4**:3068-3076

[13] Doyle AD, Montoya JH, Vojvodic A. Improving oxygen electrochemistry through nanoscopic confinement. ChemCatChem. 2015;**7**:738-742

[14] Das SK, Dutta PK. Synthesis and characterization of a ruthenium oxide-zeolite Y catalyst for photochemical oxidation of water to dioxygen. Microporous and Mesoporous Materials. 1998;**22**:475-483

[15] Zhan B-Z, White MA, Sham T-K, Pincock JA, Doucet RJ, Ramana Rao KV, et al. Zeolite-confined nano-$RuO_2$: A green, selective, and efficient catalyst for aerobic alcohol oxidation. Journal of the American Chemical Society. 2003;**125**:2195-2199

[16] Zhan B-Z, Iglesia E. $RuO_2$ clusters within LTA zeolite cages: Consequences of encapsulation on catalytic reactivity and selectivity. Angewandte Chemie. 2007;**119**:3771-3774

[17] Gong M, Li H, Liang Y, Wu JZ, Zhou J, Wang J. An advanced Ni-Fe layered double hydroxide electrocatalyst for water oxidation. Journal of the American Chemical Society. 2013;**135**:8452-8455

[18] Troup JM, Clearfield A. Mechanism of ion exchange in zirconium phosphates. 20. Refinement of the crystal structure of α-zirconium phosphate. Inorganic Chemistry. 1977;**16**:3311-3314

[19] Clearfield A, Díaz A. Zirconium phosphate nanoparticles and their extraordinary properties. In: Brunet E, Colón JL, Clearfield A, editors. Tailored Organic-Inorganic Materials. New Jersey: Wiley; 2015. pp. 1-44

[20] Clearfield A, Blessing RH, Stynes JA. New crystalline phases of zirconium phosphate possessing ion-exchange properties. Journal of Inorganic and Nuclear Chemistry. 1968;**30**:2249-2258

[21] Clearfield A, Duax WL, Medina AS, Smith GD, Thomas JR. On the mechanism of ion exchange in crystalline zirconium phosphates. Sodium ion exchange of α-zirconium phosphate. The Journal of Physical Chemistry A. 1969;**73**:3424-3430

[22] Stanley Whittingham M. Intercalation chemistry: An introduction. In: Whittingham M, Jacobson AJ, editors. Intercalation Chemistry. New York: Academic Press; 1982. pp. 1-18

[23] Alberti G, Costantino U, Gupta JP. Crystalline insoluble acid salts of tetravalent metals—XIX: $Na^+$-catalyzed $H^+$-$Mg^{2+}$ and $H^+$-$Cs^{2+}$ ion exchanges on α-zirconium phosphate. Journal of Inorganic and Nuclear Chemistry. 1974;**36**:2109-2114

[24] Alberti G, Costantino U, Gupta JP. Crystalline insoluble acid salts of tetravalent metals—XXII: Effect of small amounts of $Na^+$ on the ion exchange of alkaline earth metal ions on crystalline $Zr(HPO_4)_2 \cdot H_2O$. Journal of Inorganic and Nuclear Chemistry. 1976;**38**:1729-1732

[25] Alberti G, Constantino U. Recent progress in the intercalation chemistry of layered α-zirconium phosphate and its derivatives, and future perspectives for their use in catalysis. Journal of Molecular Catalysis. 1984;**27**:235-250

[26] Clearfield A, Duax WL, Medina AS, Smith GD, Thomas JR. On the mechanism of ion exchange in crystalline zirconium phosphates. I. Sodium ion exchange of α-zirconium phosphate. The Journal of Physical Chemistry. 1969;**78**:3424-3430

[27] Martí AA, Colón JL. Direct ion exchange of tris(2,2′-bipyridine) ruthenium(II) into an α-zirconium phosphate framework. Inorganic Chemistry. 2003;**42**:2830-2832

[28] Alberti G, Constantino U, Gill JS. Crystalline insoluble acid salts of tetravalent metals—XXIII: Preparation and main ion exchange properties of highly hydrated zirconium bis monohydrogen orthophosphates. Journal of Inorganic and Nuclear Chemistry. 1976;**38**:1733-1738

[29] Colón JL, Casañas B. Drug carriers based on zirconium phosphate nanoparticles. In: Brunet E, Colón JL, Clearfield A, editors. Tailored Organic-Inorganic Materials. New Jersey: Wiley; 2015. pp. 395-437

[30] Díaz A, David A, Pérez R, González ML, Báez A, Wark SE, et al. Nanoencapsulation of insulin into zirconium phosphate for oral delivery applications. Biomacromolecules. 2010;**11**:2465-2470

[31] Casañas-Montes B, Díaz A, Barbosa C, Ramos C, Collazo C, Meléndez E, et al. Molybdocene

dichloride intercalation into zirconium phosphate nanoparticles. Journal of Organometallic Chemistry. 2015;**791**:34-40

[32] Martí AA, Paralitici G, Maldonado L, Colón JL. Photophysical characterization of methyl viologen ion-exchanged within α-zirconium phosphate framework. Inorganica Chimica Acta. 2007;**360**:1535-1542

[33] Martí AA, Rivera N, Soto K, Maldonado L, Colón JL. Intercalation of Re(phen)$(CO)_3$Cl into zirconium phosphate: A water insoluble complex immobilized in a highly polar rigid matrix. Dalton Transactions. 2007;**17**:1713-1718

[34] Santiago M, Declet-Flores C, Díaz A, Velez MM, Bosques MZ, Sanakis Y, et al. Layered inorganic materials as redox agents: Ferrocenium-intercalated zirconium phosphate. Langmuir. 2007;**23**:7810-7817

[35] Díaz A, Saxena V, González J, David A, Casañas B, Batteas J, et al. Zirconium phosphate nano-platelets: A platform for drug delivery in cancer therapy. Chemical Communications. 2012;**48**:1754-1756

[36] Díaz A, González ML, Pérez RJ, David A, Mukherjee A, Báez A, et al. Direct intercalation of cisplatin into zirconium phosphate nanoplatelets for potential cancer nanotherapy. Nanoscale. 2013;**5**:11456-11463

[37] Santiago MB, Velez MM, Borrero S, Diaz A, Casillas CA, Hoffman C, et al. NADH electrooxidation using bis(1,10-phenanthroline-5,6-dione)(2,2′-bipyridine)ruthenium(II)-exchanged zirconium phosphate modified carbon paste electrodes. Electroanalysis. 2006;**18**:559-572

[38] Santiago MB, Daniel G, David A, Casañas B, Hernández G, Guadalupe A, et al. Effect of enzyme and cofactor immobilization on the response of ethanol amperometric biosensors modified with layered zirconium phosphate. Electroanalysis. 2010;**22**:1097-1105

[39] Rivera EJ, Barbosa C, Torres R, Grove L, Taylor S, Connick WB, et al. Vapochromic and vapoluminescent response of materials based on platinum(II) complexes intercalated into layered zirconium phosphate. Journal of Materials Chemistry. 2011;**21**:15899-15902

[40] Bermúdez RA, Colón Y, Tejada GA, Colón JL. Intercalation and photophysical characterization of 1-pyrenemethylamine into zirconium phosphate layered materials. Langmuir. 2005;**21**:890-895

[41] Rivera EJ, Figueroa C, Colón JL, Grove L, Connick WB. Room-temperature emission from platinum(II) complexes intercalated into zirconium phosphate-layered materials. Inorganic Chemistry. 2007;**46**:8569-8576

[42] Rivera EJ, Barbosa C, Torres R, Rivera H, Fachini ER, Green TW, et al. Luminescence rigidochromism and redox chemistry of pyrazolate-bridged binuclear platinum (II) diamine complex intercalated into zirconium phosphate layers. Inorganic Chemistry. 2012;**51**:2777-2784

[43] Clearfield A. Group IV phosphates as catalysts and catalyst supports. Journal of Molecular Catalysis. 1984;**27**:251-262

[44] Clearfield A, Thakur DS. Zirconium and titanium phosphates as catalysts: A review. Applied Catalysis. 1986;**26**:1-26

[45] Colón JL, Thakur DS, Yang C-Y, Clearfield A, Martin CR. X-ray phoelectron spectroscopy and catalytic activity of α-zirconium phosphate and zirconium phosphate

sulfophenylphosphonate. Journal of Catalysis. 1990;**124**:148-159

[46] Niño ME, Giraldo SA, Páez-Mozo EA. Olefin oxidation with dioxygen catalyzed by porphyrins and phthalocyanines intercalated in α-zirconium phosphate. Journal of Molecular Catalysis A: Chemical. 2001;**175**:139-151

[47] Hajipour AR, Karimi H. Zirconium phosphate nanoparticles as a remarkable solid acid catalyst for selective solvent-free alkylation of phenol. Chinese Journal of Catalysis. 2014;**35**:1136-1147

[48] Costamagna P, Yang C, Bocarsly AB, Srinivasan S. Nafion® 115/zirconium phosphate composite membranes for operation of PEMFCs above 100°C. Electrochimica Acta. 2002;**47**:1023-1033

[49] Alberti G, Casciola M. Composite membranes for medium-temperature PEM fuel cells. Annual Review of Materials Research. 2003;**33**:129-154

[50] Yang C, Srinivasan S, Bocarsly AB, Tulyani S, Benziger JB. A comparison of physical properties and fuel cell performance of Nafion and zirconium phosphate/Nafion composite membranes. Journal of Membrane Science. 2004;**237**:145-161

[51] Hou H, Sun G, Wu Z, Jin W, Xin Q. Zirconium phosphate/Nafion115 composite membrane for high-concentration DMFC. International Journal of Hydrogen Energy. 2008;**33**:3402-3409

[52] Rodgers MP, Shi Z, Holdcroft S. Ex situ characterization of composite Nafion membranes containing zirconium hydrogen phosphate. Fuel Cells. 2009;**9**:534-546

[53] Zlotorowicz A, Sunde S, Seland F. Zirconium hydrogen phosphate as an additive in electrocatalytic layers for the oxygen evolution reaction in PEM water electrolysis. International Journal of Hydrogen Energy. 2015;**40**:9982-9988

[54] Cai X, Luo Y, Liu B, Cheng H-M. Preparation of 2D material dispersions and their applications. Chemical Society Reviews. 2018;**47**:6224-6266

[55] Chen L, Sun D, Li J, Zhu G. Exfoliation of layered zirconium phosphate nanoplatelets by melt compounding. Materials and Design. 2017;**122**:247-254

[56] Sun L, Boo WJ, Sun D, Clearfield A, Sue H-J. Preparation of exfoliated epoxy/α-zirconium phosphate nanocomposites containing high aspect ratio nanoplatelets. Chemistry of Materials. 2007;**19**:1749-1754

[57] Xia F, Yong H, Han X, Sun D. Small molecule-assisted exfoliation of layered zirconium phosphate nanoplatelets by ionic liquids. Nanoscale Research Letters. 2016;**11**:348

[58] Kaschak DM, Johnson SA, Hooks DE, Kim H-N, Ward MD, Mallouk TE. Chemistry on the edge: A microscopic analysis of the intercalation, exfoliation, edge functionalization, and monolayer surface tiling reactions of α-zirconium phosphate. Journal of the American Chemical Society. 1998;**120**:10887-10894

[59] Casciola M, Alberti G, Donnadio A, Pica M, Marmottini F, Bottino A, et al. Gels of zirconium phosphate in organic solvents and their use for the preparation of polymeric nanocomposites. Journal of Materials Chemistry. 2005;**15**:4262-4267

[60] Zhou Y, Huang R, Ding F, Brittain AD, Liu J, Zhang M, et al. Sulfonic acid-functionalized α-zirconium phosphate single-layer nanosheets as a strong

solid acid for heterogeneous catalysis applications. ACS Applied Materials & Interfaces. 2014;**6**:7417-7425

[61] Zhou Y, Noshadi I, Ding H, Liu J, Parnas RS, Clearfield A, et al. Solid acid catalyst based on single-layer α-zirconium phosphate nanosheets for biodiesel production via esterification. Catalysts. 2018;**8**:17

[62] Wang L, Xu W-H, Yang R, Zhou T, Hou D, Zheng X, et al. Electrochemical and density functional theory investigation on high selectivity and sensitivity of exfoliated nano-zirconium phosphate toward lead. Analytical Chemistry. 2013;**85**:3984-3990

[63] Kim HN, Keller SW, Mallouk TE, Schmitt J, Decher G. Characterization of zirconium phosphate polycation thin films grown by sequential adsorption reactions. Chemistry of Materials. 1997;**9**:1414-1421

[64] Hunter BM, Gray HB, Müller AM. Earth-abundant heterogeneous water oxidation catalysts. Chemical Reviews. 2016;**116**:14120-14136

[65] Seh ZW, Kibsgaard K, Dickens CF, Chorkendorff I, Nørskov JK, Jaramillo TF. Combining theory and experiment in electrocatalysis: Insights into material design. Science. 2017;**355**:6321

[66] Weng B, Xu F, Wang C, Meng W, Grice CR, Yan Y. A layered $Na_{1-x}Ni_yFe_{1-y}O_2$ double oxide oxygen evolution reaction electrocatalyst for highly efficient water-splitting. Energy & Environmental Science. 2017;**10**:121-128

[67] Lu Z, Wang H, Kong D, Yan K, Hsu P-C, Zheng G, et al. Electrochemical tuning of layered lithium transition metal oxides for improvement of oxygen evolution reaction. Nature Communications. 2014;**5**:4345

[68] Oh H-S, Nong HN, Reier T, Bergmann A, Gliech M, Ferreira de Araújo J, et al. Electrochemical catalyst-support effects and their stabilizing role for $IrO_x$ nanoparticle catalysts during the oxygen evolution reaction. Journal of the American Chemical Society. 2016;**138**:12552-12563

[69] Sanchez J, Ramos-Garcés MV, Narkeviciute I, Colón JL, Jaramillo TF. Transition metal-modified zirconium phosphate electrocatalysts for the oxygen evolution reaction. Catalysts. 2017;**7**:132

[70] Mosby BM, Díaz A, Bakhmutov V, Clearfield A. Surface functionalization of zirconium phosphate nanoplatelets for the design of polymer fillers. ACS Applied Materials & Interfaces. 2014;**6**:585-592

[71] Horsley SE, Nowell DV, Stewart DT. The infrared and Raman spectra of α-zirconium phosphate. Spectrochimica Acta, Part A: Molecular and Biomolecular Spectroscopy. 1974;**30**:535-541

[72] Ramos-Garcés MV, Sanchez J, Del Toro-Pedrosa DE, Barraza Alvarez I, Wu Y, Valle E, et al. Transition metal-modified exfoliated zirconium phosphate electrocatalyst for the oxygen evolution reaction. ACS Applied Energy Materials. 2019;**2**:3561-3567. DOI: 10.1021/acsaem.9b00299